Journal of Magnetic Resonance **143,** 274–279 (2000)
doi:10.1006/jmre.1999.2005, available online at http://www.idealibrary.com on IDEAL®

Electron Paramagnetic Resonance Imaging Using Magnetic-Field-Gradient Spinning

Keiichi Ohno and Masakazu Watanabe

Department of Information Engineering, University of Industrial Technology, 4-1-1 Hashimotodai, Sagamihara, Kanagawa 229-1196, Japan

Received May 25, 1999; revised November 2, 1999

A novel X-band CW EPR imaging has been developed using magnetic-field-gradient (MFG) spinning to obtain spatial distributions of electron paramagnetic species. Spinning MFG EPR imaging for 65 projection spectra required just 55 s while conventional imaging took 11 min 40 s, that is, the acquisition time for the new system is one order of magnitude shorter than that for conventional EPR imaging. Spinning MFG EPR imaging allows one to measure reconstructed images in an interactive manner where resolution and condition can be changed quickly.

Key Words: **EPR; EPR imaging; magnetic field gradient; spinning.**

INTRODUCTION

In NMR imaging, magnetic-field-gradient (MFG) spinning where a projection spectrum is acquired once using an incident RF pulse through Fourier transformation (FT) at each MFG angle, has been developed for data acquisition. Lai *et al.* reported a microprocessor-based controller for reorienting the magnetic field gradients used in NMR imaging (*1*). It delivered 0.5 A to a gradient coil of 56 μH inductance and 9.5 Ω resistance generating an angle resolution for reorientation of 1° and a gradient of magnitude of about 40 μT/cm.

In contrast to NMR imaging, which has become a powerful tool especially in medicine, EPR imaging has not necessarily brought about any great advance because continuous-wave EPR must be used (*2, 3*). Recently, however, radiofrequency (RF) EPR imaging systems operating in the time domain have been developed successfully for biomedical research (*4–8*). On the other hand one of the authors (Ohno) has studied the development of a microcoil EPR spectroscope which is applicable to *in vivo* zeugmatographic microscopy (*9*). From the viewpoint of microscopy sensitivity must be considered the most important factor because an extremely small volume element involved in a sample provides an EPR signal per pixel. Thus an X-band CW EPR spectrometer is superior to an RF spectrometer for this purpose. In the case of the X-band time domain Fourier transformation EPR is not necessarily advantageous and thus there are alternative strategies for the development of useful CW EPR imaging. One of them is to achieve interactive EPR imaging with magnetic field modulation at 100 kHz and a phase-sensitive detector (PSD).

The procedure for EPR imaging commonly used so far is as follows. Figure 1 shows the schematic of the cross section of an object for imaging and its projection spectrum at angle θ. First, a magnetic field gradient is set and a projection spectrum is acquired with a sweep of the magnetic field range. Next the direction of the gradient is rotated by a constant angle step, and then another projection spectrum is acquired. Similar procedures are continued uniformly up to the angle π. Second, the acquired projection spectra are reconstructed to obtain the density distribution after preanalysis, using methods such as baseline corrections and integrations. Finally, the density distribution is displayed on screen as an image of the paramagnetic species. In general it takes several minutes to acquire a projection spectrum. Thus the total time necessary is 2.5 h if angular intervals of 5° are adopted (namely 36 spectra per image). This time-consuming data acquisition significantly reduces the usefulness of EPR imaging relative to NMR imaging.

Demsar and co-workers attempted to reduce the time for data acquisition using a rapid magnetic field scan taking a total time of 2 min 12 s with 19 projection spectra (*10*). The rapid magnetic field scan is generated by a saw-tooth current, which seems to necessitate a relatively wide bandwidth for obtaining good enough linearity and a considerable duration for depressing a delay of the magnetic field due to magnetic hysteresis.

Rapid spinning of the magnetic field gradient is adopted to overcome the above-mentioned problems:

$$\frac{\partial H_z}{\partial r}\,\mathbf{l}(\omega_g t) = \frac{\partial H_z(\omega_g t)}{\partial x}\,\mathbf{i} + \frac{\partial H_z(\omega_g t)}{\partial z}\,\mathbf{k} \qquad [1]$$

$$\left(\frac{\partial H_z}{\partial r}\right)^2 = \left(\frac{\partial H_z(\omega_g t)}{\partial x}\right)^2 + \left(\frac{\partial H_z(\omega_g t)}{\partial z}\right)^2. \qquad [2]$$

While r is kept constant, the direction θ of MFG rotates and the EPR signal is acquired at corresponding times for equidistant angle intervals, as shown in Fig. 1. The resultant MFG $\partial H_z/\partial r$ from $\partial H_z(\omega_g t)/\partial z$ and $\partial H_z(\omega_g t)/\partial x$, given below, is kept constant during rotation with a frequency ω_g of about 100 Hz. Here the z axis is directed along a static magnetic field, and r

1090-7807/00 $35.00

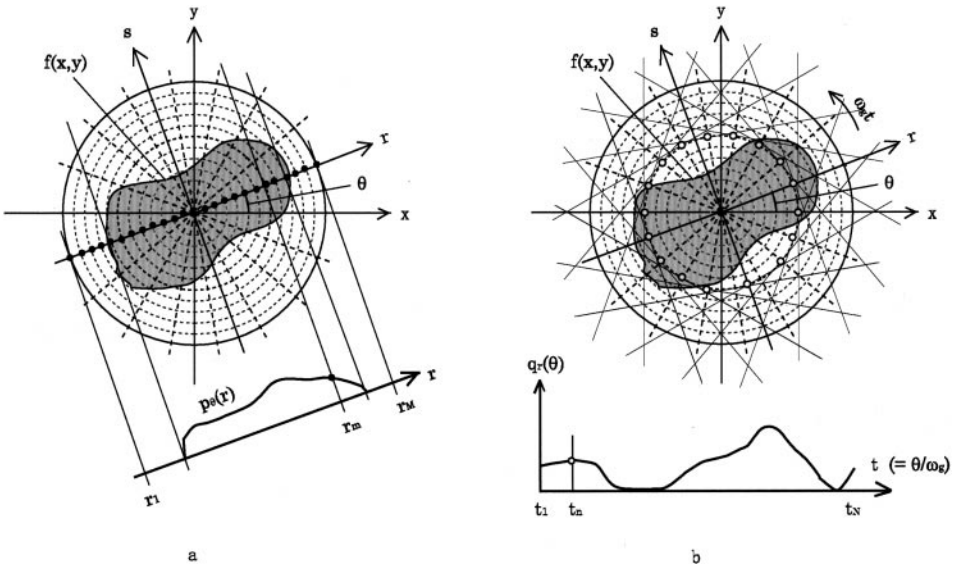

FIG. 1. Relation between a density function $f(x, y)$ and a projection spectrum at angle θ. (a) Projection spectrum $p_\theta(r)$ and (b) pinwheel-like function $q_r(\theta)$ where $\theta = \omega_g t$.

is the radial axis determined from Eqs. [1] and [2]. **i**, **k**, and **l** are, respectively, unit vectors for the x, z, and r axes, and $H_z(\omega_g t)$ is the z component of the applied magnetic field.

A set of projection spectra P is described as

$$P = \bigcup_{\theta} \{p_\theta(r) | 0 \le \theta \le 2\pi\}$$

$$= \bigcup_{0 \le \theta \le 2\pi} \sum_{r=r_1}^{r_M} \{\Delta p(r, \theta)\} \qquad [3]$$

$$= \bigcup_{r} \{q_r(\theta) | r_1 \le r \le r_M\}$$

$$= \bigcup_{r_1 \le r \le r_M} \sum_{\theta=0}^{2\pi} \{\Delta p(r, \theta)\}, \qquad [4]$$

where $p_\theta(r)$ is a projection spectrum, $q_r(\theta)$ is a pinwheel-like spectrum, and $\theta = \omega_g t$. Here $\Delta p(r, \theta)$ is a ray-sum defined as

$$\Delta p(r, \theta) = \int f(x, y) ds. \qquad [5]$$

Sampling for r is carried out at $r_1, r_2, \ldots, r_M$ where $r_m = m\Delta r$ ($m = 1, 2, \ldots, M$) as shown in Fig. 1a and for θ at $\omega_g t_1$, $\omega_g t_2, \ldots, \omega_g t_N$, where $t_n = n\Delta t/\omega_g$ ($\Delta t = \Delta\theta/\omega_g$, $n = 1, 2, \ldots, N$). The sequence of $q_r(\theta)$ corresponds to the open circles while that of $p_\theta(r)$ corresponds to the solid circles in Fig. 1. It is clear that one can rearrange the ray-sum $\Delta p(r, \theta)$'s in Eq. [4] to form $p_\theta(r)$ in Eq. [3]. Generally M is made equal to N.

After the completion of data acquisition for $q_r(\theta)$ at a certain r, the magnetic field corresponding to r is stepped with a sufficiently slow rate. The present system for the gradient requires a narrow bandwidth at a certain frequency f_g ($=2\pi\omega_g$), which is superior to the rapid magnetic-field scan method.

Figure 2a illustrates the shifts of EPR spectra from two samples located separately with positive

$$p_1^+(H_o + \Delta H_1) = p_1^-(H_o - \Delta H_1) \qquad [6]$$

$$p_2^-(H_o + \Delta H_2) = p_2^+(H_o - \Delta H_2) \qquad [7]$$

and negative MFG (denoted as $+$ and $-$). Two solid and two dotted lineshapes corresponding to $+$MFG and $-$MFG, respectively, are described as Eqs. [6] and [7]. Here H_o stands for the intrinsic resonant line, ΔH a shift of resonant line in the presence of MFG, p a projection spectrum, and 1 and 2 two samples, respectively. Assuming that the linearity of MFG is guaranteed and their absolute values are exactly the same, these lines have a reflection symmetry of about H_o, meaning that a half magnetic-field sweep is necessary and sufficient to obtain a complete projection spectrum for image reconstruction. The relation reduces the data acquisition time to half if the projection spectra in the range of $(\pi, 2\pi)$ are taken to be the same as the corresponding ones in the range of $(0, \pi)$ except for the directions.

If the number of projection spectra is set to be odd as shown in Fig. 2b, the projection spectrum in the range $(\pi, 2\pi)$ can be taken to be that at a bisector of the gradient between the two sequential orientations. For example, the gradient of No. 6 corresponds to that of No. 1′, the bisector between No. 1 and

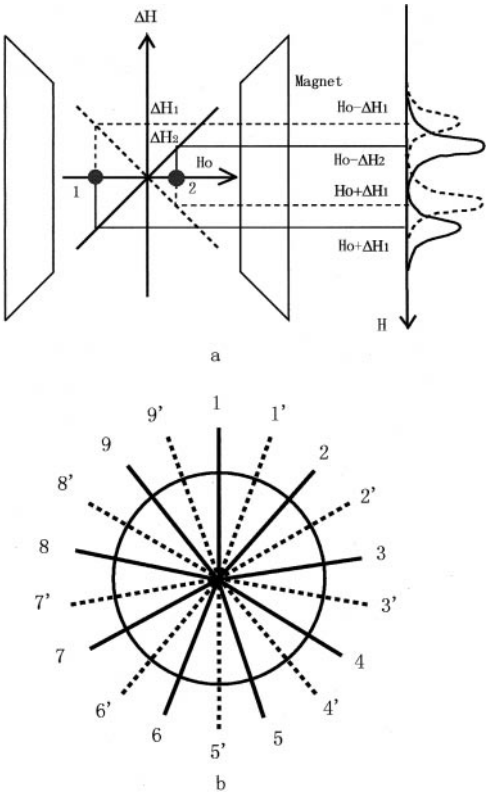

FIG. 2. Relation of projection spectra and magnetic field gradients. (a) Projection spectra from samples 1 and 2 in the presence of positive and negative magnetic field gradients; p, projection spectrum; ΔH, shift of EPR line. (b) Reflection symmetry among projection spectra in the case of an odd number of MFG orientations.

No. 2. This results in considering the number of total projection spectra spreading over $(0, 2\pi)$ equal to the number of projection spectra in the range of $(0, \pi)$ which should be approximately the number of data points in general. In the present paper we use an odd number of projection spectra spreading over $(0, 2\pi)$.

For convenience we call the minimum procedure for acquiring a sequence of projection spectra spreading over $(0, \pi)$ without any accumulation a cycle. The duration for one cycle is also called the time resolution. The purpose of the present research is to reduce the time resolution to that of one FID in the FT EPR, which is generally very noisy, but is accumulated, resulting in an excellent spectrum. To obtain a noise-free image one will need to accumulate the projection spectra sufficiently. The reduction of the time resolution will lead to a more interactive EPR imaging system.

EXPERIMENTAL

Two small single crystals of lithium phthalocyanine (LiPc) (about $0.2 \times 0.2 \times 0.5$ mm^3) were fixed on the outside surface of a glass tube at a distance of 2.95 mm. The LiPc single crystal was used as a sample giving a dot in an image. After the sample was inserted into another thick sample tube, it was sealed off under evacuation to less than 10^{-3} mm Hg (0.133 Pa). An apparently single line was observed to consist of three components, of which two have oxygen-dependent linewidths (2.5–3 μT at a microwave power of 7 μW and 23.5 μT at a power of 2.6 mW), and the other has no such dependency (0.1 mT at a power of 124 mW). In the present experiment, however, an incident microwave power of several milliwatts was used so that there is no problem in regarding them as a single line with a linewidth of about 0.1 mT (*11–14*).

Projection spectrum measurement was carried out with a Bruker CW EPR spectrometer ESP-300E modified with an anti-Helmholtz coil pair (copper wire 54 turns, wire diameter 0.75 mm, inner diameter 47.5 mm, outer diameter 63.3 mm) for $\partial \mathrm{H}_z(\omega_g t)/\partial z$ and a figure-8 Helmholtz coil pair (copper wire 40 turns, wire diameter 0.9 mm, inner diameter 37.5 mm, outer diameter 55 mm) for $\partial \mathrm{H}_z(\omega_g t)/\partial x$. They were fed currents by two fast-response bipolar power supplies (Kikusui PBX20-5; transient time 0 to 5 A, 100 μs) to generate the rapid spinning MFG, $\partial H_z/\partial r$. The assembly consisted of two coils each of 0.49 mH inductance and 1.0 Ω resistance and two coil pairs of 0.45 mH inductance and 0.94 Ω resistance at each pair for $\partial H_z(\omega_g t)/\partial z$ and $\partial H_z(\omega_g t)/\partial x$, respectively.

A personal computer, PC1 (Gateway 2000, Pentium 130 MHz), controlled the power supplies through a DA converter (Interface IBX-3309, eight 12-bit channels, conversion time 10 μs) as shown in Fig. 3. A 100-kHz magnetic field modulation of less than 48 μT was used to avoid line distortion due to an extremely narrow intrinsic linewidth of LiPc.

During the rotation of the MFG with an angle velocity of ω_g, EPR signals were acquired through an AD converter (Interface IBX-3161, four 8-bit channels, conversion time 0.05 μs) at each time interval (Δt) corresponding to each angle interval $(\Delta\theta)$. After the data acquisition $q_r(\theta)$ in a static magnetic field

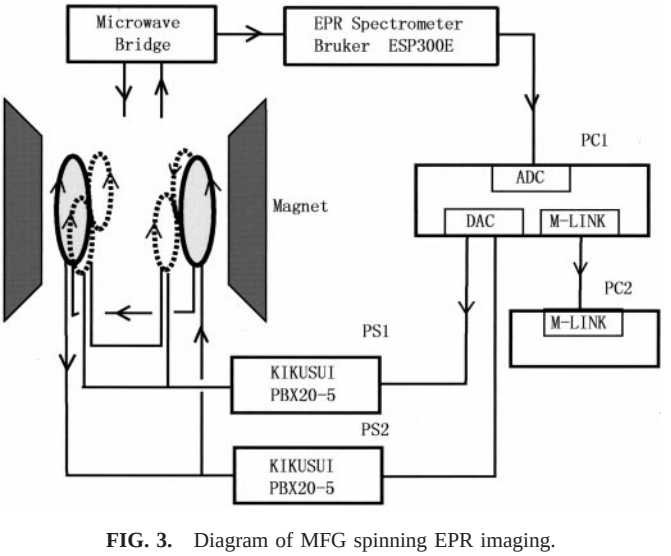

FIG. 3. Diagram of MFG spinning EPR imaging.

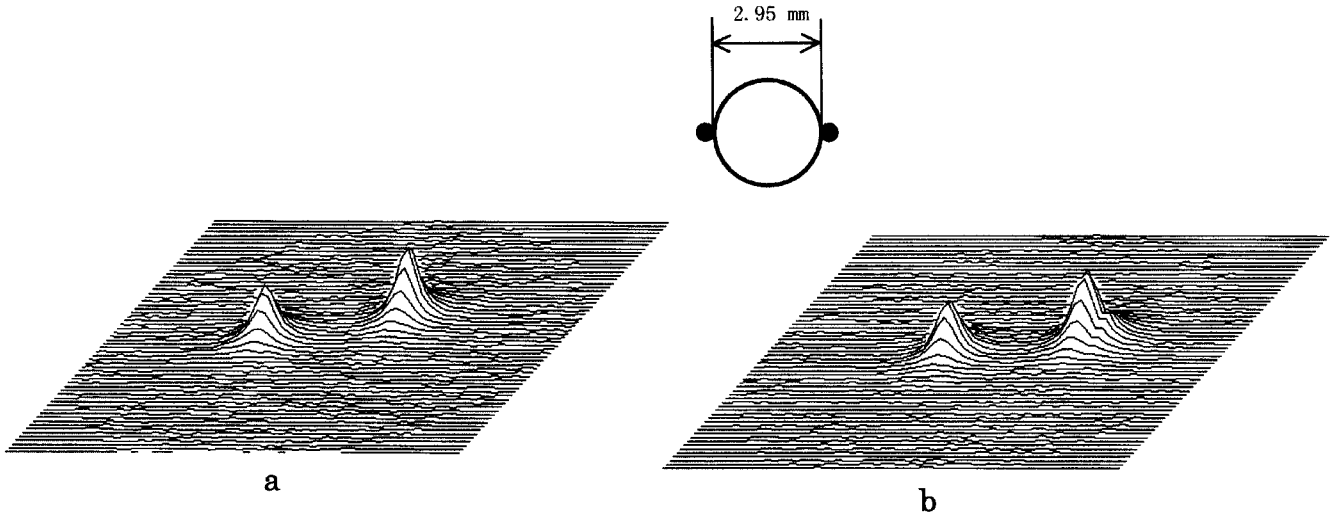

FIG. 4. Reconstructed images of LiPc single crystals. (a) Image obtained with the conventional method and (b) image obtained with the MFG spinning method under a spinning rate of 20 Hz. Inset shows a phantom with two tiny single crystals of LiPc separated by 2.95 mm. Both particles were attached to a quartz sample tube. In both cases the number of data points and that of projection spectra was 65. The time constant of the PSD was 0.01 ms.

r_m, the magnetic field was stepped to r_{m+1} and a similar data acquisition was performed. When data acquisitions had been completed for all data points in the range from r_1 to r_M, the stored data $q_r(\theta)$'s were instantaneously transferred to another personal computer, PC2 (ES-COM el5133pci1250c8/8, Pentium 133 MHz), through two memory-link interface boards (Interface PCI-4913) connected with PC1. Then projection spectra $p_\theta(r)$ for all angles of the MFG were extracted from the stored data $q_r(\theta)$. Figure 3 depicts a diagram of spinning MFG EPR imaging.

A filtered back-projection algorithm was used to reconstruct images from the projection spectra. To compare the spinning MFG EPR imaging with conventional methods, an EPR imaging measurement using a static MFG was made with the same sample.

RESULTS AND DISCUSSION

In Fig. 4a a 2-D relative spin distribution of LiPc is shown in perspective from the conventional static MFG. It took a

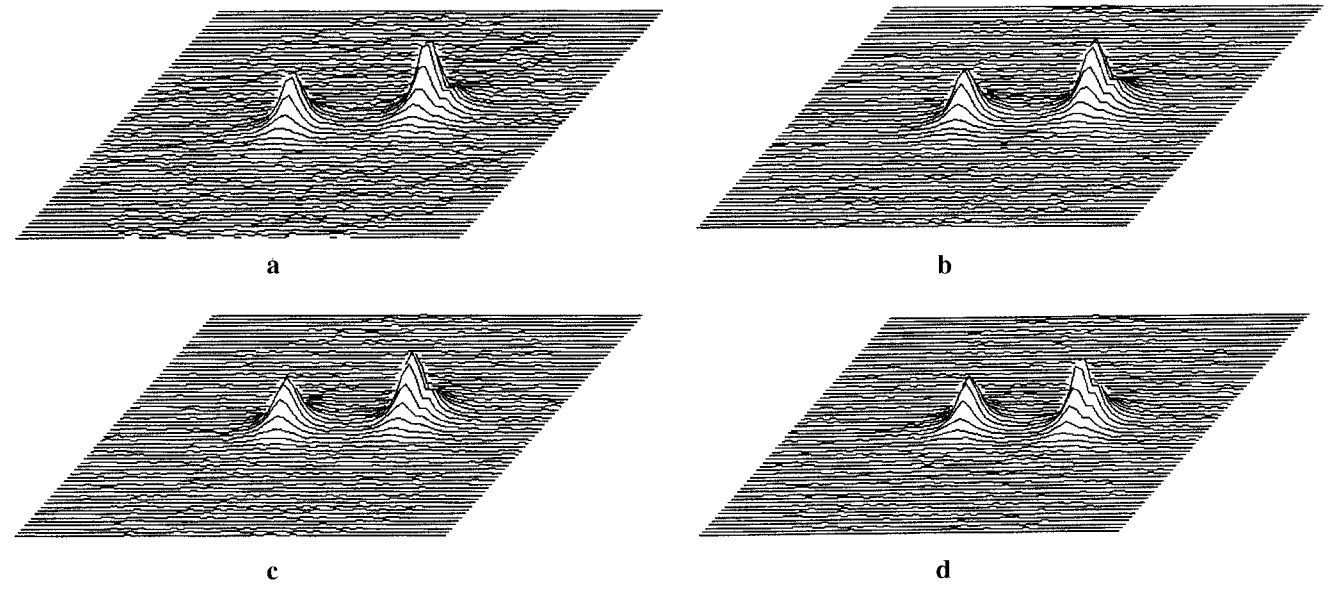

FIG. 5. Frequency dependence of reconstructed images. (a) 10 Hz, (b) 20 Hz, (c) 30 Hz, and (d) 60 Hz. The number of data points and that of projection spectra was 65. The time constant of the PSD was 0.01 ms.

minimum of 11 min 40 s to perform the whole time course for an image. Figure 4b shows a similar image obtained using MFG spinning. The number of accumulations was 16 and the number of projection spectra was 65. In this case a minimum of 55 s was required, so the time resolution to carry out one cycle was calculated to be about 3.4 s at 20 Hz. To compare the two methods, the signal-to-noise ratio (SNR) for both images was made approximately equal (47.8 and 46.8 dB, respectively). The MFG spinning EPR imaging requires only 1/10 of the time required for conventional techniques. It is important, however, to keep in mind that these acquisition times might increase to 10 times longer if the concentration of the paramagnetic species (LiPc) was 1/10 that of the present one. In contrast, the acquisition times might reduce to 1/10 shorter when the concentration increased to 10 times the present one. Therefore the comparison of the duration of 55 s with Demsar's results of 2.2 min is of little significance because the experiments were performed with different samples and SNRs.

Note here that the direction of a line through the two peaks in Fig. 4a does not coincide with that in Fig. 4b. The angle difference of 5° may originate from the phase delay of the latter signal. The phase delay is due mainly to the impedances of the MFG coils. The remaining part of the phase delay may be due to extra time needed to execute a program driving the DAC and ADC interfaces in PC1. Figure 5 shows the frequency dependence of reconstructed images using spinning MFG EPR imaging. As the frequency increases from 10 to 60 Hz the phase delay increases from 3° to 16°. Simultaneously the distances of the two peaks were kept almost constant, indicating that spinning MFG EPR imaging will be useful up to 60 Hz. This fact suggests that the frequency characteristics of the spinning MFG system will be achievable at several hundreds of Hertz with the improvement of the coil system and the extra time required for driving the DAC and ADC interfaces.

Figure 6 shows the effect of data points on the acquisition times and resolution of reconstructed images with projection spectra of 33, 65, and 129. Acquisition times for 30 Hz were 19, 38, and 71 s, respectively.

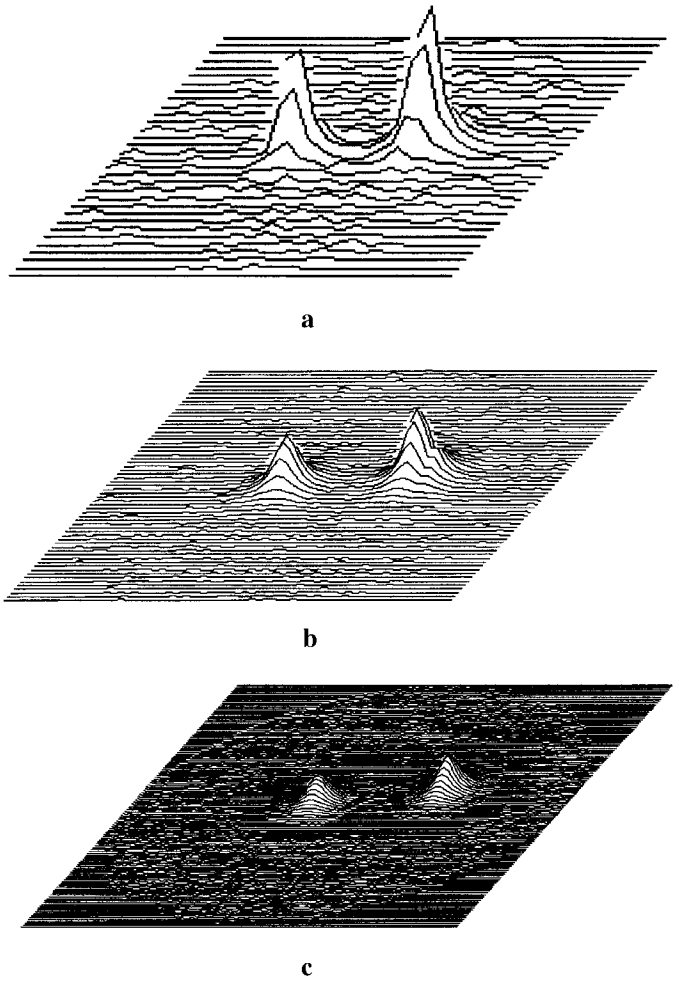

FIG. 6. Data-point dependence of reconstructed images. The number of data points was (a) 33 for an acquisition time of 19 s, (b) 65 for 38 s, and (c) 129 for 1 min 11 s. The spinning rate was 30 Hz.

CONCLUSION

A novel method of EPR imaging which requires shorter data acquisition times has been developed successfully by the use of MFG spinning for obtaining distributions of paramagnetic species. The rate of MFG spinning to observe the reconstructed images could increase up to 60 Hz except for a little rotation. The time resolution of the EPR imaging system to perform one cycle was simply estimated to be about 1.3 s at 60 Hz. The total time required to obtain images with the same SNR for the present system was reduced to one order of magnitude shorter than that for the conventional technique.

The improvement of the coil assembly and the software driving the DAC and ADC interfaces will enable one to use an MFG spinning at several hundreds of Hertz and to realize a more interactive EPR imaging system. The short time resolution will make it possible to select interactively appropriate resolution, S/N ratio, and total data acquisition time.

Furthermore, in *in vivo* EPR imaging for living animals, pulsatory motion may occur and generate noisy and regular signals, but the time course of images may be meaningful during each period. In these cases the short time resolution will allow one to measure the variations and/or distributions of paramagnetic species interested by use of a synchronous trigger with the pulsation.

REFERENCES

1. C.-M. Lai, J. W. Shook, and P. C. Lauterbur, *Chem. Biomed. Environ.* **9**(1), 1–27 (1979).
2. G. R. Eaton and S. S. Eaton, Pulsed EPR imaging, *in* "EPR Imaging and In Vivo EPR" (G. R. Eaton, S. S. Eaton, and K. Ohno, Eds.), pp. 73–78, CRC Press, Boca Raton (1991).
3. G. R. Eaton and S. S. Eaton, EPR imaging, *in* "Foundation of

Modern EPR" (G. R. Eaton, S. S. Eaton, and K. M. Salikhov, Eds.), pp. 684–694, World Scientific, Singapore (1997).

4. J. Bourg, M. C. Krishna, J. B. Mitchell, R. G. Tschudin, T. J. Pohida, W. S. Friauf, P. D. Smith, J. Metcalfe, F. Harrington, and S. Subramanian, *J. Magn. Reson. B* **102,** 112–115 (1993).
5. A. Coy, N. Kaplan, and P. T. Callanghan, *J. Magn. Reson. A* **121,** 201–205 (1996).
6. R. Murugesan, J. A. Cook, N. Devasahayam, M. Afeworki, S. Subramanian, R. G. Tschudin, J. A. Larsen, J. B. Mitchell, A. Russo, and M. C. Krishna, *Magn. Reson. Med.* **38,** 409–414 (1997).
7. M. Alecci, J. B. Brivati, G. Placidi, and A. Sotgiu, *J. Magn. Reson.* **130,** 272–280 (1998).
8. S. Subramanian, R. Murugesan, N. Devasahayam, J. A. Cook, M. Afeworki, T. Pohida, R. G. Tschudin, J. B. Mitchell, and M. C. Krishna, *J. Magn. Reson.* **137,** 379–388 (1999).
9. Y. Morita and K. Ohno, *J. Magn. Reson. A* **102,** 344–347 (1993).
10. F. Demsar, T. Walczak, P. D. Morse II, G. Bačić, Z. Zolnai, and H. M. Swartz, *J. Magn. Reson.* **76,** 224–231 (1988).
11. P. Turek, J.-J. Andre, and J. Simon, *Solid State Commun.* **63**(8), 741–744 (1987).
12. A. I. Smirnov, S.-W. Norby, T. Walczak, K. J. Liu, and H. M. Swartz, *J. Magn. Reson. B* **103,** 95–102 (1994).
13. F. Bensebaa and J.-J. André, Effect of oxygen on phthalocyanine radicals, *J. Phys. Chem.* **96,** 5739–5745 (1992).
14. F. Bensebaa, P. Petit, and J.-J. André, *Synth. Metals* **52,** 57–69 (1992).